Solution Structure of the Aminofluorene-Stacked Conformer of the *syn* [AF]-C^8-dG Adduct Positioned at a Template-Primer Junction[†,‡]

Bing Mao,[§] Zhengtian Gu,[§] Andrey Gorin,[§] Brian E. Hingerty,[∥] Suse Broyde,[⊥] and Dinshaw J. Patel*[,§]

Cellular Biochemistry and Biophysics Program, Memorial Sloan-Kettering Cancer Center, New York, New York 10021, Life Sciences Division, Oak Ridge National Laboratory, Oak Ridge, Tennessee 37831, and Biology Department, New York University, New York, New York 10003

Received September 5, 1997[⊗]

ABSTRACT: A solution structural study has been undertaken on the aminofluorene-C^8-dG ([AF]dG) adduct located at a single strand−double strand d(A1-A2-C3-[AF]G4-C5-T6-A7-C8-C9-A10-T11-C12-C13)·d(G14-G15-A16-T17-G18-G19-T20-A21-G22) 13/9-mer junction (designated [AF]dG 13/9-mer) using proton−proton distance and intensity restraints derived from NMR data in combination with a computational protocol, which includes intensity refinement. This single strand−double strand junction models one arm of a replication fork composed of a 13-mer template strand, which contains the [AF]dG modification site, and a 9-mer primer strand, which has been elongated up to, but not including, the modified guanine. The NMR data establish that the duplex segment retains a minimally perturbed B-DNA conformation including Watson−Crick hydrogen-bonding at the junctional dC5·dG22 base pair. The NMR spectra are consistent with the guanine ring of the [AF]dG4 adduct adopting a *syn* glycosidic torsion angle and being displaced into the major groove with the adjacent dC3 residue displaced into the minor groove. Such a base displacement of the modified guanine is accompanied by stacking of one face of the fluorene ring of [AF]dG4 with the dC5·dG22 base pair, while the other face of the flourene ring is stacked with the purine ring of the nonadjacent dA2 residue in the intensity-refined solution structures of the [AF]dG 13/9-mer. A comparison of structural features of the C^8-[AF]dG adduct (this study) with those of the (+)-*trans*-*anti*-N^2-[BP]dG adduct [Cosman et al. (1995) *Biochemistry 34,* 15334−15350] in the same 13/9-mer junctional sequence context has identified common features associated with the alignment of the modified guanine adducts at the template-primer junction. Thus, despite differences in the covalent linkage site for the C^8-[AF]dG and (+)-*trans*-*anti*-N^2-[BP]dG adducts, one face of the aromatic ring of the carcinogen stacks over the junctional base pair and in so doing displaces the modified guanine in a *syn* alignment into the major groove. These results lend credence to earlier proposals that such an adduct alignment may represent a common mutagenic conformer at a template-primer junction associated with a replication fork.

The mutagenic and tumorigenic properties of the aromatic amines 2-aminofluorene (AF) and 2-acetylaminofluorene (AAF) have been the subject of great interest for decades. The most important covalent adduct formed following metabolic activation of both these substances is the deacetylated AF one to C^8 of guanine (*1*). It is the only adduct resulting directly from reaction of activated AF with DNA, and *in vivo*, the major AAF adduct to guanine C^8 is largely deacetylated. Consequently, it is especially important to delineate the structural properties of the [AF]dG adduct in order to elucidate the relationship to mutagenesis. Since mutations can occur during replication at a DNA single strand−duplex junction, an understanding of structure in this sequence context is particularly relevant to mutagenicity. A single strand−duplex junction is a model for an arm of a replication fork, with one strand representing the parent template strand and the second one representing the elongating daughter containing the next to be elongated primer residue. A template containing the [AF]dG modification, with daughter strand elongated up to the lesion site so that the modified base would be the next to be replicated, is a key structure for understanding what the replication machinery would encounter once it reaches the damaged base.

In previous research (*2*), the solution structure of the major adduct of the tumorigenic (+)-*anti*-benzo[*a*]pyrene−diol−epoxide (BPDE), the (+)-t*rans*-*anti* adduct to guanine N^2 (designated [BP]dG), has been elucidated at a primer-template junction by a combination of high-resolution NMR and molecular mechanics computations. The present study concerns the structure of the C^8-[AF]dG adduct **1** (Figure 1A) in the same sequence context **2** (Figure 1B) previously employed for the N^2-[BP]dG adduct. We wish to ascertain if common structural features are shared between these pairs of adducts that have been paradigms for the aromatic amine and polycyclic aromatic hydrocarbon families of carcinogens, at this model replication intermediate, and to relate the observed structural features to mutagenic outcome.

MATERIALS AND METHODS

Materials. *N*-Acetoxy-2-acetylaminofluorene (AAAF) was purchased from the Chemsyn Science Laboratories. The

[†] This research is supported by NIH Grant CA-49982 to D.J.P., by NIH Grants CA-28038, CA75449, and RR-06458, and DOE Grant DE-FG02-90ER60931 to S.B., and by DOE Contract DE-AC05-960R22464 with Lockheed Martin Energy Research.

[‡] The coordinates of the [AF]dG 13/9-mer duplex have being deposited in the Brookhaven Protein Data Base (file name 1AX7).

[§] Memorial Sloan-Kettering Cancer Center.

[∥] Oak Ridge National Laboratory.

[⊥] New York University.

[⊗] Abstract published in *Advance ACS Abstracts,* November 15, 1997.

S0006-2960(97)02206-X CCC: $14.00

deoxyoligonucleotides d(A-A-C-G-C-T-A-C-C-A-T-C-C) and d(G-G-A-T-G-G-T-A-G) were synthesized on an Applied Biosystems Model 392 DNA synthesizer and purified by reverse-phase HPLC.

Preparation of Adduct. The d(A-A-C-G-C-T-A-C-C-A-T-C-C) sequence was reacted with excess AAAF in 2 mM citrate buffer as reported previously (*3*). The [AAF]dG-modified 13-mer strand was purified by reverse-phase HPLC on a C18 ODS-Hypersil semipreparative column (Keystone Scientific Inc.). The [AAF]dG 13-mer was converted into the [AF]dG 13-mer by dissolving in 1 M NaOH containing 0.3% (v/v) 2-mercaptoethanol for 45 min at room temperature followed by purification by reverse-phase HPLC as outlined above. The [AF]dG 13-mer was desalted on Sephadex G-25 and converted to its sodium form on a Dowex 50 × 8 cation exchange resin column. The [AF]dG modified 13-mer strand was next annealed with the complementary d(G-G-A-T-G-G-T-A-G) 9-mer strand at 70 °C, and the stoichiometry was followed by monitoring single proton resonances in both strands.

NMR Experiments. One- and two-dimensional NMR spectra were recorded on approximately 5 mg of [AF]dG 13/9-mer in 0.6 mL, 0.1 M NaCl, 10 mM phosphate, and pH 7.0 aqueous buffer. The NOESY spectrum (150 ms mixing time) of the [AF]dG 13/9-mer in H_2O buffer at 1 °C was collected using a jump-return pulse for solvent suppression. NOESY spectra (50, 80, 120, 160, 200, and 300 ms mixing times) were collected to provide NOE buildup data and assignment in D_2O buffer at 25 °C. In addition, a NOESY spectrum (150 ms mixing time) of the [AF]dG 13/9-mer was also collected in D_2O buffer at 1 °C.

Heteronuclear $^1H-^{13}C$ and $^1H-^{31}P$ spectra on the [AF]dG 13/9-mer were collected as reported previously (*4*, *5*). The measurement of NOE intensity-based distance bounds used for the generation of DUPLEX-based starting structures of the [AF]dG 13/9-mer are similar to those outlined in the Methods section of the preceeding paper on the [AF]dG·del(−2) 12/10-mer (*6*).

Molecular Mechanics. The DUPLEX-based molecular mechanics calculations (*7*) are the same as outlined in the Methods section of earlier papers from our laboratory (*4*, *8*). Computations were carried out at the Department of Energy's National Energy Research Supercomputer Center and the National Science Foundation's San Diego Supercomputer Center.

Relaxation Matrix Refinement. The final unrestrained energy-minimized structure of the [AF]dG 13/9-mer obtained following completion of the first stage DUPLEX calculations was used as the starting point for subsequent refinement using X-PLOR-based intensity refinement (*9*) as described in the Methods section of the preceeding paper on the [AF]dG·del(−2) 12/10-mer (*6*).

The relaxation matrix was set up for the nonexchangeable protons with the exchangeable imino, amino, and hydroxyl protons exchanged for deuterons. A total of 950 nonexchangeable intensity restraints from the NOESY data sets at five mixing times in D_2O (190 intensities per mixing time) and 188 nonexchangeable distance restraints were included in the calculations. Diheral angle restraints (corresponding to B-DNA) were included with a very low weight of 5 kcal rad^{-2} and restricted to residues dT6-dC13 and dG14-dA21 duplex segments separated by one base pair from the [AF]dG4 lesion site.

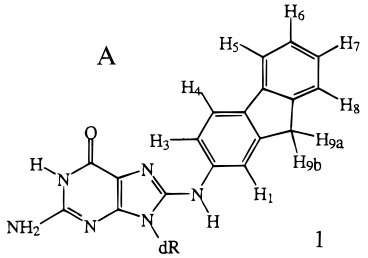

1

B

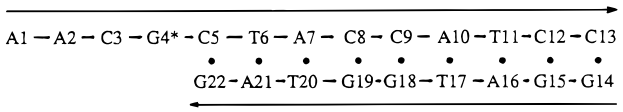

2

FIGURE 1: (A) Schematic of the [AF]dG adduct **1**. (B) Schematic and numbering system of the [AF]dG 13/9-mer **2**.

Six intensity refinement trials were performed with the DUPLEX-based starting structure heated in each trial to 1000 K through the assignment of an arbitrary Maxwell−Boltzmann velocity distribution corresponding to a temperature of 1000 K. Then, after 2.4 ps dynamics evolution at that temperature, the system was gradually cooled to 300 K during 7.2 ps with the "heat bath" method, and equilibrated at 300 K for 2.4 ps. After equilibration, the coordinates were subjected to energy minimization to a gradient of 0.1 kcal mol^{-1} $Å^{-1}$.

RESULTS

Exchangeable Nucleic Acid Protons. The exchangeable proton NMR spectrum (10−14.5 ppm) of the [AF]dG 13/9-mer **2** (Figure 1B) in H_2O buffer solution, pH 7.0, at 1 °C exhibits eight well-resolved resonances between 12.5 and 14.0 ppm and two upfield shifted resonances at 12.01 and 10.80 ppm (Figure 2A). These imino protons have been assigned following analysis of the 150-ms mixing time of NOESY spectrum based on established assignment procedures (reviewed in refs 10 and 11). The connectivities between adjacent base pairs in the [AF]dG 13/9-mer from the dC5·dG22 pair located at the single strand−duplex junction to the dC13·dG14 pair located toward the opposite end of the helix are traced in the expanded NOESY (150 ms mixing time) contour plot of the symmetrical 11.5−14.0 ppm imino proton region in Figure 3C. An expanded plot of the 150 ms mixing time NOESY spectrum of the [AF]dG 13/9-mer correlating NOE connectivities between the imino protons (11.5−14.0 ppm) and the base and amino protons (5.2−8.5 ppm) is plotted in Figure 3B. The observed NOE patterns establish Watson−Crick base pairing at all dA·dT pairs (thymine imino to adenine H2 protons) and at all dG·dC pairs (guanine imino to cytosine amino and H5 protons), including the junctional dC5·dG22 base pair (peaks A, A′, and B, Figure 2B).

The imino proton of dG22, located at the junction site, sharpens and upfield shifts (12.01 ppm) upon adduct formation relative to the control 13/9-mer (*2*). In addition, we observe intermolecular NOEs between the imino proton of dG22 and protons on the fluorenyl ring (numbered cross-peaks in Figure 3A,B).

The upfield shifted imino proton at 10.80 ppm is assigned to [AF]dG4 based on a very weak NOE to its own averaged

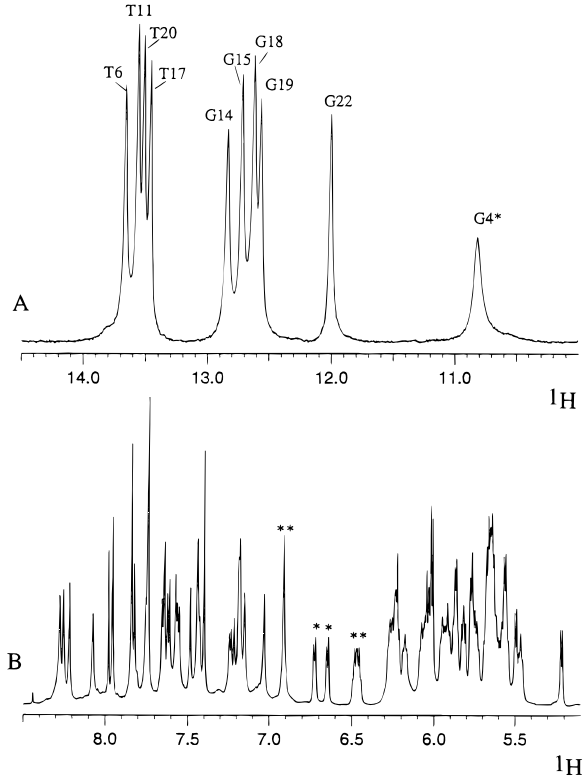

FIGURE 2: (A) Imino proton spectra (10.0−14.5 ppm) of the [AF]dG 13/9-mer in H_2O buffer at 1 °C and (B) nonexchangeable proton spectra (5.1−8.5 ppm) of the [AF]dG 13/9-mer in D_2O buffer at 25 °C. The buffer was 0.1 M NaCl, 10 mM phosphate, and 0.1 mM EDTA at pH 7.0. The imino proton assignments are shown over the resonances in the spectrum in panel A. The AF protons are marked by asterisks in panel B.

amino protons at 6.39 ppm and an exchange cross-peak with the H_2O resonance in the adduct duplex. We do not detect NOEs between the imino proton of [AF]dG4 and other imino and nonexchangeable protons in the NOESY contour plots of the adduct duplex.

The exchangeable imino and amino proton chemical shifts for the central d(A1-A2-C3-[AF]G4-C5-T6-A7)·d(T20-A21-G22) segment of the [AF]dG 13/9-mer at 1 °C are listed in Table 1 and for the entire adduct containing single strand−duplex junction in Supplementary Table S1 (Supporting Information).

Nonexchangeable Nucleic Acid Protons. The base and sugar H1′ nonexchangeable proton spectrum region (5.1−8.5 ppm) of the [AF]dG 13/9-mer in D_2O buffer, pH 7.0, at 25 °C is shown in Figure 2B. It exhibits well-resolved, narrow resonances for both the single strand and duplex segments in the [AF]dG 13/9-mer. Nonexchangeable proton assignments are based on an analysis of through-space NOESY data sets (50 and 300 ms mixing times at 25 °C and 150 ms mixing time at 1 °C) and through-bond COSY and TOCSY data sets (40 and 80 ms spin lock times) at 25 °C based on established assignment procedures (reviewed in refs 10 and 11).

The expanded NOESY (300 ms mixing time) contour plot establishing sequential connectivities between the base protons (6.8−8.4 ppm) and the sugar H1′ and cytosine H5 protons (5.1−6.4 ppm) of the [AF]dG 13/9-mer in D_2O buffer, pH 7.0, at 25 °C is plotted in Figure 4A. The corresponding expanded NOESY (150 ms mixing time) contour plot in D_2O buffer at 1 °C is plotted in Figure 4B.

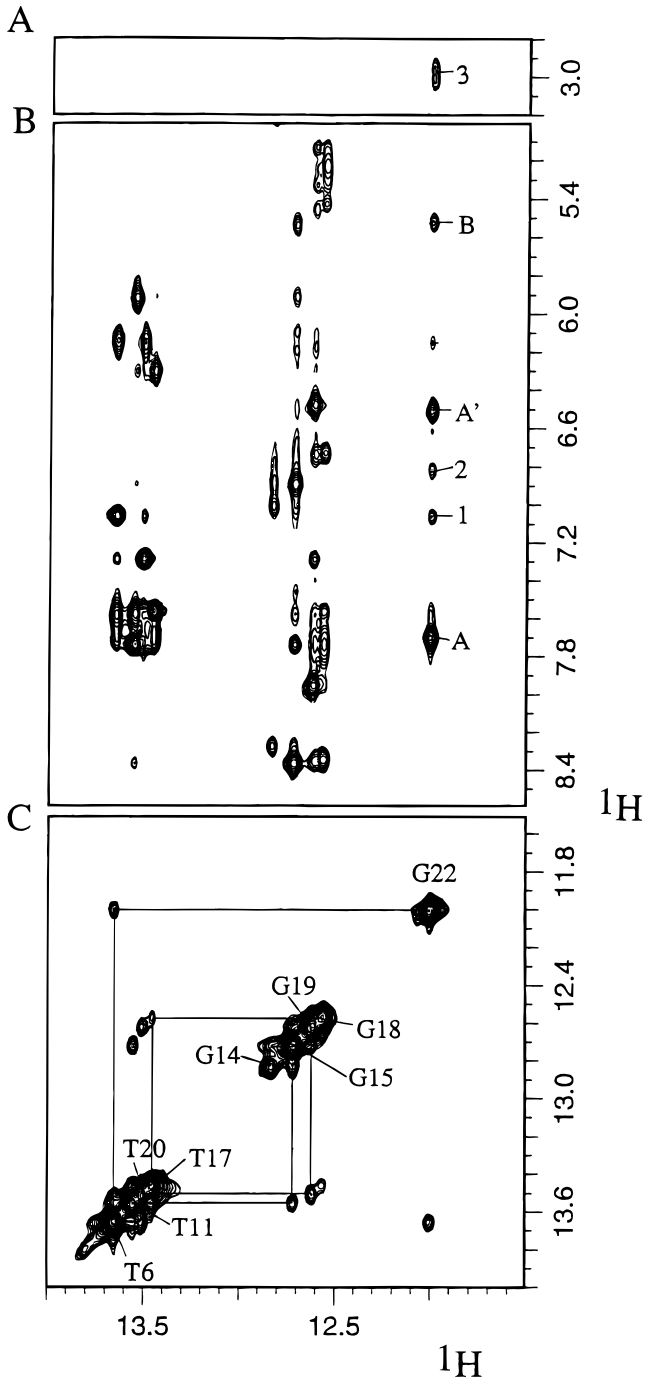

FIGURE 3: Expanded NOESY (150 ms mixing time) contour plots of the [AF]dG 13/9-mer in H_2O buffer at 1 °C. (A) NOE connectivities between the imino protons (11.5−14.0 ppm) and the AF methylene protons (2.8−3.2 ppm). The carcinogen−DNA cross-peak 3 is assigned as follows: 3, G22(NH1)-AF(H9a,b). (B) NOE connectivities between the imino protons (11.5−14.0 ppm) and the base and amino proton regions (5.0−8.6 ppm). The NOE cross-peaks involving the imino protons are labeled in the figure as follows: A, A′, G22(NH1)-C5(NH_2-4b,e); B, G22(NH1)-C5(H5). The carcinogen−DNA NOE cross-peaks 1−2 are assigned as follows: 1, G22(NH1)-AF(H1); 2, G22(NH1)-AF(H3,4). (C) NOE connectivities in the symmetrical (11.5−14.0 ppm) region. The imino proton assignments are labeled along the diagonal. The lines trace the NOE connectivities between adjacent base pairs starting at dG22 toward one end of the helix and proceeding to dG14 toward the other end of the helix.

The AF(H3) and AF(H4) protons, which are superpositioned at 6.90 ppm, as well as A2(H1′) and C5(H5) protons, which are superpositioned at ≈ 5.54 ppm in the contour plot at 25

Table 1: Proton and Phosphorus Chemical Shifts of the d(A1-A2-C3-[AF]G4-C5-T6-A7)·d(T20-A21-G22) Segment of the [AF]dG 13/9-mer[a]

	G(NH1)/T(NH3)	C(NH_2-4)	H8/H6	H5/H2/CH_3	H1′	H2′	H2″	H3′	H4′	^{31}P[b]
dA1			7.73		5.80	1.55	1.88	4.52	4.05	−4.59
dA2			7.94	7.39	5.54	2.47	2.09	4.55	4.19	−3.83
dC3			7.60	6.00	6.00	1.98	2.40	4.67	4.05	−3.59
[AF]dG4	10.80	6.39			6.07	3.72	2.36	4.91	4.41	−3.15
dC5		7.70,[c] 6.50[d]	7.74	5.55	5.85	2.10	2.43	4.83	4.27	−4.31
dT6	13.65		7.44	1.60	5.60	2.12	2.43	4.83	4.27	−4.31
dA7			8.25	7.39	6.17	2.68	2.85	5.00	4.41	−4.21
dT20	13.52		7.14	1.30	5.57	1.96	2.30	4.80	4.12	−4.21
dA21			8.07	7.20	5.94	2.61	2.78	4.98	4.33	−4.13
dG22	12.01		7.47		5.67	2.48	2.34	4.66	4.14	

[a] All chemical shifts are in ppm. Exchangeable proton chemical shifts at 1 °C. Nonexchangeable proton and phosphorus chemical shifts at 25 °C. [b] ^{31}P chemical shift corresponds to residue *n* in *n*-^{31}P-(*n* + 1) step. [c] Hydrogen-bonded amino proton. [d] Exposed amino proton.

°C in Figure 4A, are resolved in the corresponding contour plot at 1 °C in Figure 4B. The base to sugar H1′ proton connectivities are traced from dA1 to dA7 along the modified strand (solid line, Figure 4) and from dT20 to dG22 along the complementary strand (dashed line, Figure 4) in the contour plot of the [AF]dG 13/9-mer at 25 and 1 °C. The interruption in the tracing at the dC3-[AF]dG4 step on the modified strand is due to the absence of a purine H8 proton following AF modification at the C^8 position of dG4 in the adduct duplex. Weak interresidue cross-peaks are also observed for the d(A1-A2-C3) segment (Figure 4) on the modified strand of the [AF]dG 13/9-mer. These base and sugar H1′ proton assignments have been confirmed by cross-checks in other regions of the NOESY contour plot (Figure 5A), as well as from COSY (Figure 5B) and TOCSY contour plots to yield a complete set of sugar H2′, H2″, H3′, and H4′ proton assignments in the [AF]dG 13/9-mer. The chemical shifts of the nonexchangeable nucleic acid protons for the d(A1-A2-C3-[AF]G4-C5-T6-A7)·d(T20-A21-G22) segment of the [AF]dG 13/9-mer are listed in Table 1 and for the entire adduct containing single strand−duplex junction in Table S1 (Supporting Information).

We observe an inversion in the characteristic H2′ and H2″ sugar cross-peak patterns at the lesion site with the H2′ proton chemical shift (3.72 ppm) of [AF]dG4 shifting dramatically downfield in the NOESY (Figure 5A) and COSY (Figure 5B) contour plots of the [AF]dG 13/9-mer. Such large downfield guanine sugar H2′ proton chemical shifts have been associated with *syn* alignments of modified guanine residues in DNA helices (*2*, *4*, *5*, *12*, *13*).

Aminofluorene Protons in the [AF]dG 13/9-mer. The nonexchangeable fluorene protons were assigned from an analysis of the through-space NOE patterns and through-bond coupling connectivities in the [AF]dG 13/9-mer. These nonexchangeable fluorene proton chemical shifts are compared in Figure 6 to the corresponding values in duplexes containing [AF]dG positioned opposite dC where the AF ring either intercalates into the helix (*14*) or is looped out into solution (*15*). The aromatic fluorene ring protons resonate between 6.4 and 7.2 ppm in the [AF]dG 13/9-mer (closed circles, Figure 6). A similar upfield shift is observed for the fluorene protons in the AF-intercalated conformer (open circles, Figure 6) of the [AF]dG·dC 12-mer duplex (*14*) while they are shifted downfield in the AF-external conformer (open squares, Figure 6) of the [AF]dG·dC 12-mer duplex (*15*). The chemical shifts of the fluorene protons in the [AF]-dG 13/9-mer are listed in the caption to Figure 6.

Intermolecular NOEs in the [AF]dG 13/9-mer. A set of intermolecular AF-DNA NOE cross-peaks have been identified in the NOESY spectra of the [AF]dG 13/9-mer and are listed in Table 2. Some of these intermolecular AF-DNA NOE cross-peaks in the [AF]dG 13/9-mer are labeled by numbers in the expanded NOESY plots of the exchangeable protons in H_2O solution (Figure 3) and nonexchangeable protons in D_2O solution (Figures 4A, B and 5A), and their assignments are listed in the figure captions.

The intermolecular NOE patterns define the alignment of the fluorene ring at the junction site in the [AF]dG 13/9-mer. The AF(H1) proton exhibits NOEs to the dA2(H1′), dA2(H8), dC5(H1′), and dC5(H5) protons, while the AF(H3) and AF(H4) protons exhibit NOEs to the minor groove sugar protons of dA2(H2″), [AF]dG4(H1′), and dC5(H1′) in the [AF]dG 13/9-mer. These NOE cross-peaks suggest that the aminofluorene ring is stacked over the dC5·dG22 base pair with the AF(H3,H4)-containing edge directed toward the minor groove in the adduct at the single strand−duplex junction.

Carbon Spectra. The expanded contour plot of a natural abundance proton−carbon HMQC correlation experiment that correlates the H1′ and C1′ chemical shifts of individual residues for the [AF]dG 13/9-mer in D_2O buffer at 25 °C is plotted in Figure 7A. The carbon resonances are assigned on the basis of the known H1′ proton assignments in the adduct single strand−duplex junction. The C1′ chemical shift assignments for residues in the d(A2-C3-[AF]G4-C5-T6)·d(A21-G22) segment in the [AF]dG 13/9-mer are labeled in Figure 7A. We note that the C1′ chemical shift of [AF]dG4 (86.81 ppm) is downfield relative to other assignable dG residues in this segment of the single strand−duplex junction (Figure 7A). It has been previously shown that downfield sugar C1′ carbon chemical shifts (that can range up to 5 ppm) are observed for DNA residues adopting *syn* glycosidic torsion angles provided that they retain C2′-*endo* sugar pucker geometries (*16*, *17*). We detect a strong coupling cross-peak between the H1′ (6.07 ppm) and H2′ (3.72 ppm) protons of [AF]dG4 (Figure 5B) placing this sugar within the C2′-*endo* range.

Phosphorus Spectra. The proton-decoupled phosphorus spectrum of the [AF]dG 13/9-mer has been recorded in D_2O buffer at 25 °C. The phosphorus resonances are dispersed over a 1.5 ppm range with two resonances shifted to low field of the −3.5 to −4.5 ppm spectral region. The phosphorus resonances have been assigned from an analysis of the proton detected phosphorus−proton heteronuclear correlation experiment with the expanded contour plot shown

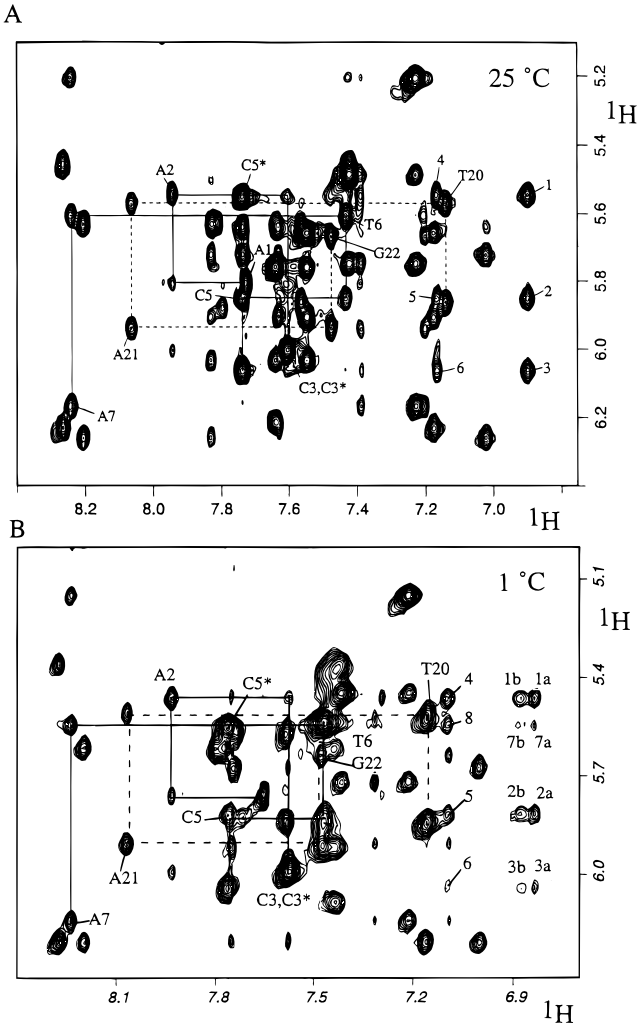

FIGURE 4: Expanded NOESY contour plots establishing distance connectivities between the base (purine H8 and pyrimidine H6) protons (6.75−8.4 ppm) and the sugar H1′ and cytosine H5 protons (5.1−6.4 ppm) of the [AF]dG 13/9-mer in D_2O buffer at (A) 25 °C (300 ms mixing time) and (B) 1 °C (150 ms mixing time). The NOE connectivities between the base and their own and 5′-flanking sugar H1′ protons from dA1 to dA7 on the modified strand are shown by solid lines and from dT20 to dG22 on the unmodified partner strand are shown by dashed lines. The assignments label the base to their own sugar H1′ NOEs, while the deoxycytidine H6-H5 NOEs are designated by asterisks. Note that the NOE cross-peak at the dC3-[AF]dG4 step is missing because of the absence of an H8 proton for [AF]dG4. The NOESY spectrum measured at 1 °C (panel B) yields well-resolved cross-peaks for the AF(H3) and AF(H4) protons and for the A2(H1′) and C5(H5) protons while each set are superpositioned in the NOESY spectrum recorded at 25 °C (panel A). The carcinogen−DNA NOE cross-peaks are assigned as follows: 1, AF(H3,H4)-A2(H1′); 2, AF(H3,H4)-C5-(H1′); 3, AF(H3,H4)-[AF]G4(H1′); 4, AF(H1)-A2(H1′); 5, AF(H1)-C5(H1′); 6, AF(H1)-[AF]G4(H1′); 7, AF(H3,4)-C5(H5); 8, AF(H1)-C5(H5), with a and b (in panel B) indicating resolved AF(H3) and AF(H4) protons, respectively.

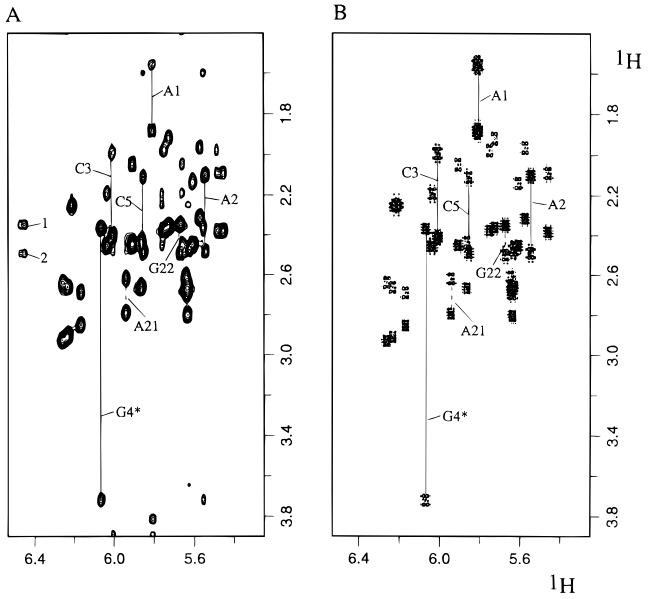

FIGURE 5: (A) Expanded NOESY (300 ms mixing time) contour plot of the [AF]dG 13/9-mer in D_2O buffer at 25 °C showing NOEs between the sugar H1′ protons (5.25−6.5 ppm) and H2′,H2″ protons (1.4−3.9 ppm). (B) Expanded phase-sensitive COSY contour plot of the [AF]dG 13/9-mer in D_2O buffer at 25 °C establishing coupling connectivities between the H1′ protons (5.25−6.5 ppm) and H2′,H2″ protons (1.4−3.9 ppm). In both panels A and B, the H2′ and H2″ protons of dA1, dA2, dC3, [AF]dG4, dC5, dA21, and dG22 are connected by lines and labeled. The H2′ protons resonate upfield of the H2″ protons for the majority of these residues except for [AF]dG4, dA2, and dG22 where the H2″ protons resonate upfield of the H2′ proton. The carcinogen−DNA NOE cross-peaks are assigned as follows: 1, AF(H6,H7)-G22(H2″) and 2, AF(H6,H7)-G22(H2′).

in Figure 7B. Several phosphorus resonance can be correlated to the 5′-linked H3′ proton and the 3′-linked H4′ and H5′,5″ protons. The phosphorous chemical shifts for the dC3-[AF]dG4 (−3.60 ppm) and [AF]dG4-dC5 (−3.16 ppm) steps are shifted to low field of the −3.8 to −4.6 ppm unperturbed phosphodiester backbone chemical shift range.

Molecular Mechanics Computations. The search strategy employed began with a B-DNA (*18*) central d(A1-A2-C3-[AF]G4-C5-T6)·d(A21-G22) base pair segment of the [AF]dG 13/9-mer. The computations were guided by the intermolecular AF-DNA restraints listed in Table 2. The AF-DNA orientation space was searched with 16 energy minimization trials in which the linkage torsion angles α′ ([AF]dG4(N^9)-[AF]dG4(C^8)-[AF](N)-[AF](C^2)) and β′ ([AF]dG4(C^8)-[AF]-(N)-[AF](C^2)-[AF](C^1)) were each started at 0°, 90°, 180°, and 270° in all combinations. In these trials, the DUPLEX hydrogen-bond penalty function (*7*) for Watson−Crick base pairing was utilized at all base pairs, since the NMR data indicated that these hydrogen bonds were present.

Three of the 16 computed structures exhibited good fit to the NMR data and had low energies. These three structures of the lesion site are superimposed and shown in Figure S1 (Supporting Information). The structure with lowest energy was embedded into an energy-minimized B-form 13/9-mer and reminimized with all restraints. Subsequently, the hydrogen-bond penalty function and the distance restraints were released with energy minimization in one step, yielding the final unrestrained structure with the C^9 containing edge of the aminofluorene ring directed toward the major groove.

Relaxation Matrix Refinement. The DUPLEX-based unrestrained structure of the [AF]dG 13/9-mer duplex served as the starting structure for intensity-based refinements using the XPLOR-based computational protocol outlined in the Methods section. An ensemble of six structures of the [AF]-dG 13/9-mer obtained following intensity refinement demonstrated an improved correspondence with experimental intensity and distance restraint data sets. The number of distance bounds violated by more than 0.2 Å decreased from 31 after first-stage DUPLEX refinement to 10 after second-stage intensity refinement (with 4−5 violations in the d(A1-

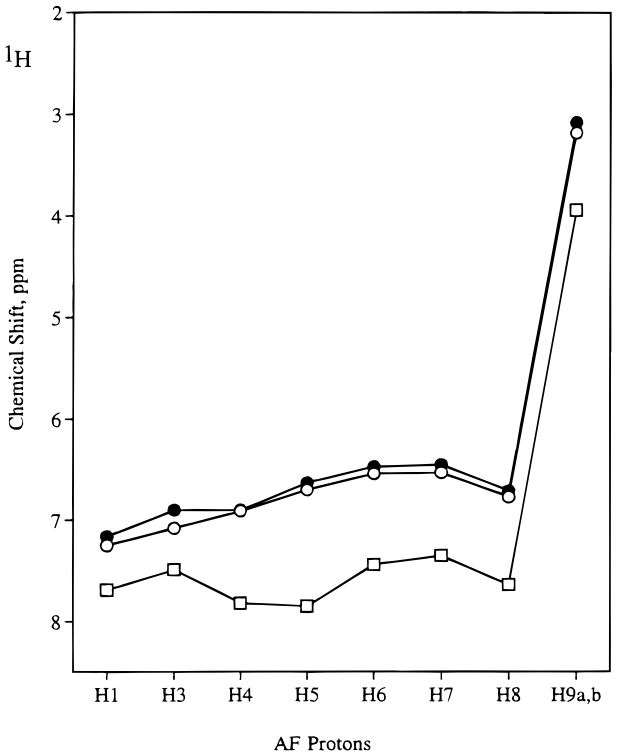

FIGURE 6: Plot comparing the aminofluorene ring proton chemical shifts in the [AF]dG 13/9-mer (closed circles) with the corresponding chemical shifts for AF-intercalated conformer (open circles) and the AF-external conformer (open squares) in the [AF]dG·dC 12-mer duplex (*14*, *15*). The chemical shift values for the aminofluorene protons in the [AF]dG 13/9-mer are AF(H1), 7.16 ppm; AF(H3), 6.90 ppm; AF(H4), 6.90 ppm; AF(H5), 6.63 ppm; AF(H6), 6.47 ppm; AF(H7), 6.45 ppm; AF(H8), 6.71 ppm; AF(H9a,b), 3.08 ppm; AF(NH), 8.61 ppm.

A2-C3-[AF]G4-C5-T6)·d(A21-G22) 6/2-mer segment with respect to different structures in the ensemble). Further, the NMR R-factor ($R_{1/6}$) improved from an initial value of 7.0% to 2.3% on proceeding from the DUPLEX-based to intensity refinement-based structures. The intensity refinement based structures of the [AF]dG 13/9-mer exhibit good stereochemistry with rmsd values for bond length, bond angle, and improper dihedral angle violations of 0.012 ± 0.001 Å, 3.15 ± 0.05°, and 0.47 ± 0.03°, respectively (Table 3).

The rmsd values between the six intensity-refined structures and the initial structure of the [AF]dG 13/9-mer is 2.8 ± 0.4 Å for all heavy atoms and 1.8 ± 0.2 Å for the 5/2-mer d(A2-C3-[BP]G4-C5-T6)·d(A21-G22). At the same time, the intensity-refined structures converge with pairwise rmsd values in the set being 2.07 ± 0.33 Å for all heavy atoms, 1.48 ± 0.33 Å for the heavy atoms of the d(A2-C3-[BP]G4-C5-T6)·d(A21-G22) 5/2-mer segment, and 1.03 ± 0.31 Å for the heavy atoms of 5/2-mer excluding backbone (Table 3).

The superpositioned view of six intensity-refined structures of the d(A1-A2-C3-[AF]G4-C5-T6)·d(A21-G22) segment of the [AF]dG 13/9-mer is plotted in Figure 8A. A corresponding view looking down the helix axis of the d(A2-C3-[AF]-G4-C5)·dG22 segment is plotted in Figure 8B.

Solution Structures. A view normal to the helix axis and looking into the major groove of the central d(A1-A2-C3-[AF]G4-C5-T6)·d(A21-G22) segment of a representative structure from the ensemble of six intensity-refined structures of the [AF]dG 13/9-mer is shown in Figure 9A. The corresponding structure for the entire duplex in stereo is shown in Figure 10. The covalently linked fluorene ring stacks over the dC5·dG22 base pair in one direction, and the purine ring of the unpaired dA2 residue stacks in the other direction. The guanine ring of the *syn* [AF]dG4 is displaced into the major groove while the dC3 residue is positioned outside the helix (Figure 9A).

Table 2: Comparison of Experimental Intermolecular Distance Restraints with Those Observed for the Intensity-Refined Structures of the [AF]dG 13/9-mer

	interproton distances (Å)	
	exptl bounds	observed
Exchangeable Protons (Carcinogen−DNA)		
AF(H1)-G22(NH1)	3.0−6.0	5.4 ± 0.2
AF(H3,H4)-G22(NH1)	3.0−6.0	6.3 ± 0.3
AF(H9a,H9b)-G22(NH1)	3.0−6.0	4.2 ± 0.1
AF(NH)-*G4(H1′)	2.3−3.6	2.4 ± 0.2
AF(NH)-C5(H5)	3.2−4.9	5.2 ± 0.5
AF(NH)-*G4(H2″)	3.0−4.6	4.2 ± 0.4
AF(NH)-*G4(H2′)	3.3−5.0	4.6 ± 0.1
AF(NH)-A2(H2′)	3.0−6.0	3.1 ± 0.4
AF(NH)-A2(H2″)	3.0−6.0	3.0 ± 0.3
Nonexchangeable Protons (Carinogen−DNA)		
AF(H1)-A2(H1′)	2.8−4.5	3.8 ± 0.1
AF(H3)-A2(H1′)	2.6−4.0	3.1 ± 0.1
AF(H4)-A2(H1′)	2.5−4.3	3.1 ± 0.1
AF(H3,H4)-A2(H2″)	2.5−5.0	3.3 ± 0.1
AF(H3,H4)-A2(H2′)	3.0−6.0	4.1 ± 0.1
AF(H1)-A2(H8)	3.9−5.9	4.0 ± 0.1
AF(H8)-A2(H2)	3.7−5.8	5.0 ± 0.1
AF(H5)-A2(H2)	3.8−5.8	4.5 ± 0.1
AF(H3,H4)-A2(H8)	3.5−5.3	5.5 ± 0.1
AF(H3)-*G4(H2′)	3.5−6.5	6.3 ± 0.1
AF(H1)-*G4(H1′)	3.2−4.8	4.0 ± 0.1
AF(H3)-*G4(H1′)	2.5−4.6	4.0 ± 0.1
AF(H3)-*G4(H2″)	3.0−6.0	5.6 ± 0.1
AF(H1)-C5(H5)	3.0−5.0	4.0 ± 0.1
AF(H3)-C5(H5)	5.0−6.5	5.9 ± 0.1
AF(H1)-C5(H1′)	2.5−4.5	4.4 ± 0.1
AF(H3)-C5(H1′)	2.7−4.1	3.3 ± 0.1
AF(H6,H7)-G22(H2′)	2.2−5.0	4.2 ± 0.1
AF(H8)-G22(H1′)	3.8−5.8	5.5 ± 0.1
AF(H8)-G22(H2′)	3.3−5.0	4.8 ± 0.1
AF(H8)-G22(H2″)	3.5−5.4	5.4 ± 0.1
AF(H6,H7)-G22(H8)	3.0−6.0	4.2 ± 0.1
AF(H6,H7)-G22(H3′)	3.0−6.0	5.6 ± 0.1
AF(H6,H7)-G22(H2″)	2.0−4.0	3.1 ± 0.1
AF(H6,H7)-G22(H1′)	2.2−5.0	3.6 ± 0.1

A view looking down the helix axis of the central d(A2-C3-[AF]G4-C5)·d(G22) segment of the NMR energy-minimized structures of the [AF]dG 13/9-mer are shown in Figure 9B. This view emphasizes the overlap geometry between the fluorene ring system and the flanking dC5·dG22 base pair and the dA2 residue. The long axis of the fluorene ring of AF is approximately parallel to the long axis of the dC5·dG22 base pair (Figure 9B).

The carcinogen−base linkage site for the [AF]dG4 residue is defined by the torsion angles α′ ([AF]dG4(N^9)-[AF]dG4-(C^8)-[AF](N)-[AF](C^2)) = 230.7 ± 27.5° and β′ ([AF]dG4-(C^8)-[AF](N)-[AF](C^2)-[AF] (C^1)) = 10.5 ± 22.8° in the intensity-refined structures of the [AF]dG 13/9-mer. The glycosidic torsion angles and sugar pseudorotation angles for the d(A1-A2-C3-[AF]G4-C5-T6)·d(A21-G22) segment of the six intensity-refined structures of the [AF]dG 13/9-mer duplex are listed in Table S2 (Supporting Information). The χ(O4′-C1′-N9-C4) glycosidic torsion angle of the [AF]dG4 residue adopts a value of χ = 30.8 ± 21.4° in the

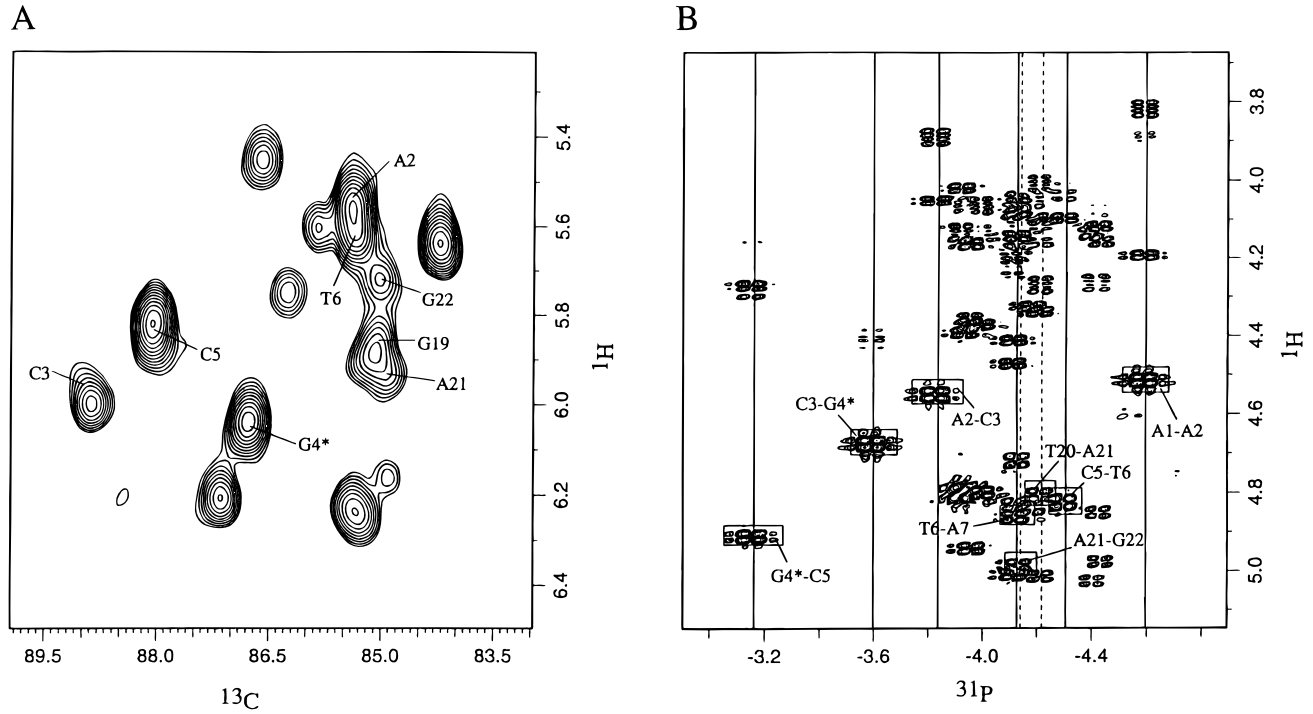

FIGURE 7: (A) Expanded contour plot of $^{1}H-^{13}C$ heteronuclear multiple-quantum coherence (HMQC) experiment on the [AF]dG 13/9-mer in D_2O buffer at 25 °C. The C1′ assignments are marked for residues in the d(A2-C3-[AF]G4-C5-T6)·d(A21-G22) segment. (B) Expanded contour plot of the proton-detected phosphorus-proton heteronuclear correlation experiment on the [AF]dG 13/9-mer in D_2O buffer at 25 °C. The phosphorus assignments are listed for steps centered about the lesion site. The correlation cross-peaks between the phosphorus and its 5′-flanking sugar H3′ protons are boxed.

Table 3: NMR Refinement Statistics for the [AF]dG 13/9-mer

NMR distance restraints	
total no. of distance restraints	188
central segment distance restraints[a]	93
NMR intensity restraints	
total intensity restraints	190 per mixing time
central segment intensity restraints	93 per mixing time
structure statistics	
NMR *R*-factor ($R_{1/6}$)	0.023 ± 0.001
rmsd of NOE violations	0.078 ± 0.003
no. of NOE violations >0.2 Å in the entire 13/9-mer	10.0 ± 0.9
no. of NOE violations >0.2 Å in the 6/2 mer region of 13/9-mer[d]	4.8 ± 0.8
deviations from the ideal geometry	
bond length (Å)	0.012 ± 0.001
bond angle (deg)	3.15 ± 0.05
impropers (deg)	0.47 ± 0.03
pairwise rmsd (Å) among the six refined structures (heavy atoms only)	
entire 13/9-mer	2.07 ± 0.33
5/2-mer region[b]	1.48 ± 0.33
5/2-mer region[b] without backbone	1.03 ± 0.31

[a] The d(A1-A2-C3-[AF]G4-C5-T6)·d(A21-G22) segment. [b] The d(A2-C3-[AF]G4-C5-T6)·d(A21-G22) segment.

syn range while the pseudorotation **P** value of dA2 is distinct and exhibits a value of 12.3 ± 8.9° (Table S2).

DISCUSSION

Spectral Quality. We observe well-resolved exchangeable (Figure 2A) and nonexchangeable (Figure 2B) proton resonances for the [AF]dG 13/9-mer of a quality comparable to those observed previously for the control 13/9-mer spectrum (*2*). In addition, well-resolved NOE connectivities involving exchangeable (Figure 3) and nonexchangeable (Figure 4) protons for the single-strand and duplex segments

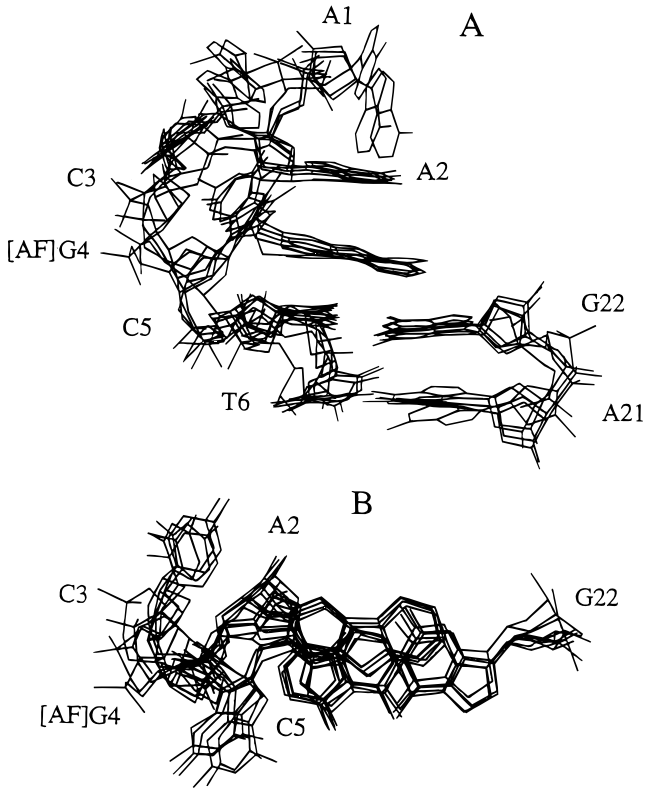

FIGURE 8: (A) Superposition of the d(A1-A2-C3-[AF]G4-C5-T6)·d(A21-G22) segments of the six intensity-refined structures of the [AF]dG 13/9-mer looking into the major groove and normal to the helix axis. (B) Superposition of the d(A2-C3-[AF]G4-C5)·dG22 segments of the six intensity-refined structures of the [AF]dG 13/9-mer looking down the helix axis.

were observed in the NOESY data sets of the [AF]dG 13/9-mer. The assignments of these proton resonances and the

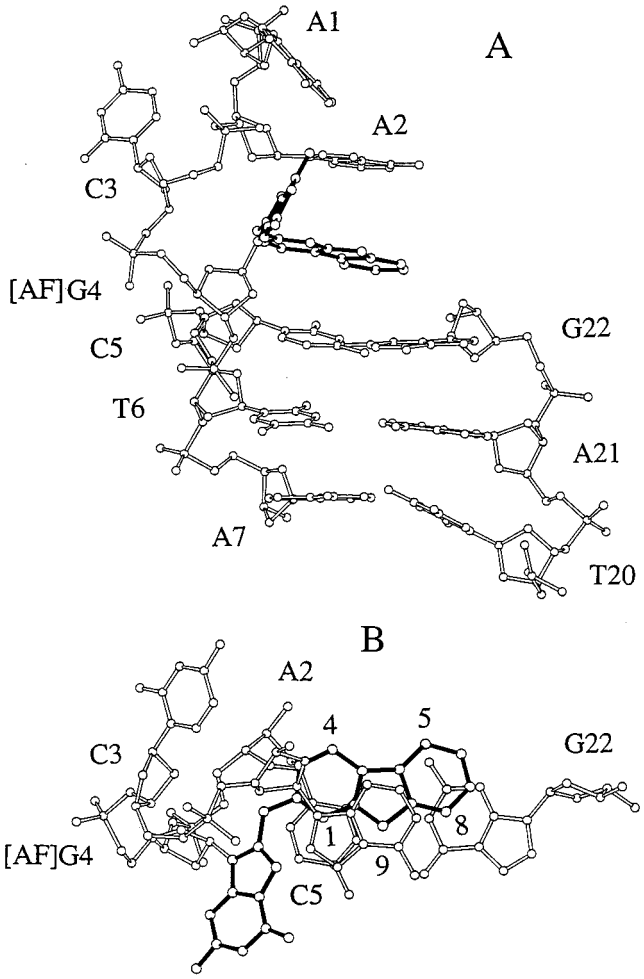

FIGURE 9: Representative structure of the [AF]dG 13/9-mer selected from the ensemble of six intensity refined structures. (A) View looking into the major groove and normal to the helix axis of the central d(A1-A2-C3-[AF]G4-C5-T6-A7)·d(T20-A21-G22) segment. The AF ring system is shown in darkened bonds and is stacked over the dC5·dG22 base pair. The modified dG4 base is displaced into the major groove. (B) View looking down the helix axis for the d(A2-C3-[AF]G4-C5)·d(G22) segment of the [AF]dG 13/9-mer. Figures were prepared using Molscript VI.1 (*35*).

identifications of the intermolecular AF-DNA NOEs provide sufficient restraints (Table 2) to define the solution structure at the junction site of the [AF]dG 13/9-mer.

Single Strand−Duplex Junction Site. The key structural features of the [AF]dG 13/9-mer solution structure are (a) the modified guanine adopts a *syn* alignment, (b) the duplex segment of the [AF]dG 13/9-mer remains in an unperturbed B-DNA conformation with all Waston-Crick alignments retained, including the dC5·dG22 base pair, (c) the fluorene ring stacks with the dC5·dG22 base pair located at the junction site, and (d) the modified guanine is displaced into the major groove.

The assignment of a *syn* glycosidic torsion angle at the [AF]dG4 lesion site has been based on the downfield shifts observed for the H2′ proton (3.72 ppm) (Figure 5) and the C1′ carbon (86.81 ppm) (Figure 7A) in spectra of the [AF]dG 13/9-mer. The downfield shift of the H2′ proton probably reflects in-plane ring current contributions from the modified guanine ring of the adduct in a *syn* alignment. Such a large downfield H2′ proton shift has been reported for the benzo[*a*]pyrene-N^2-guanine adduct positioned at a duplex−single strand junction where the *syn* alignment at the adduct site was independently established from the strong NOE between the base H8 and its own H1′ proton (*19*) in short mixing time NOESY spectra of the adduct containing duplex (*2*).

The modified guanine is displaced into the major groove in the intensity-refined structures of the [AF]dG 13/9-mer (Figures 8 and 9). The imino proton of [AF]dG4 is not basepaired consistent with its upfield chemical shift (10.80 ppm) and its rapid exchange with solvent water. The dC3 residue is displaced into the minor groove, resulting in a loss of stacking interactions between this residue and the neighboring residues dA2 and [AF]dG4 in the intensity-refined structures of the [AF]dG 13/9-mer. This is consistent with the absence or very weak sequential NOEs (Figure 4) within the dA2-dC3-[AF]dG4 segment extending from the junction site.

The observed NOE cross-peaks between the upfield shifted dG22 imino proton and the amino and H5 protons of dC5 (Figure 3B) establishes that the dC5·dG22 base pair maintains a Waston-Crick alignment in the [AF]dG 13/9-mer. The imino proton resonance of dG22 sharpens and exchanges slowly with solvent upon AF-modification (compare Figure 1A of ref 2 with Figure 2A in the present study), indicating that the terminal dC5·dG22 base pair is stabilized on going from the control 13/9-mer to the [AF]dG 13/9-mer. This can be explained by the stacking interaction between the fluorene ring of [AF]dG4 and the dC5·dG22 base pair in the intensity-refined structures of the [AF]dG 13/9-mer.

One face of the fluorene ring is stacked with the dC5·dG22 base pair and on the other face with the purine ring of dA2 in the intensity-refined structures of the [AF]dG 13/9-mer. We observe large upfield shifts for the imino proton (12.01 ppm) of dG22 and amino protons (6.50 and 7.70 ppm for the exposed and hydrogen-bonded amino protons, respectively) of dC5 of the [AF]dG 13/9-mer (Table 1) relative to their corresponding values in the control 13/9-mer (*2*). This observation is consistent with the observed stacking interaction between the fluorene ring and the dC5·dG22 base pair and the dA2 base in the refined structure of the [AF]dG 13/9-mer. The aromatic protons of the fluorene ring in the [AF]-dG 13/9-mer resonate in the same range (6.4−7.5 ppm, Figure 6) as those observed for the AF-intercalated conformer in the [AF]dG·dC 12-mer (*14*), consistent with the stacking of the AF ring between adjacent base pairs/bases in both systems. The stacking of the purine ring of the dA2 residue with the AF ring in the intensity-refined structures of the 13/9-mer (Figures 8 and 9) is supported by the observation of several intermolecular NOEs between the base protons (H8 and H2) of dA2 and the NH and aromatic protons of AF in the [AF]dG 13/9-mer (Table 2).

The observed downfield phosphorus chemical shifts for the [AF]dG4-dC5 step and, to a lesser extent, for the dC3-[AF]dG4 step on the modified strand of the [AF]dG 13/9-mer (Figure 7B) must reflect the conformational perturbations associated with accomodation of the [AF]dG adduct at the single strand−duplex junction. There is a sufficient spread in the values of the backbone torsion angles on either side of the [AF]dG adduct to preclude attempts to correlate the downfield shifted phosphorus chemical shifts with specific changes in the backbone torsion angles (B_I and B_{II} conformations) as has been proposed in the literature (*20*).

We did not use coupling constant data as restraints during the computations. A list of sugar pseudorotation pucker (**P**) parameters and glycosidic torsion (χ) angles for residues at

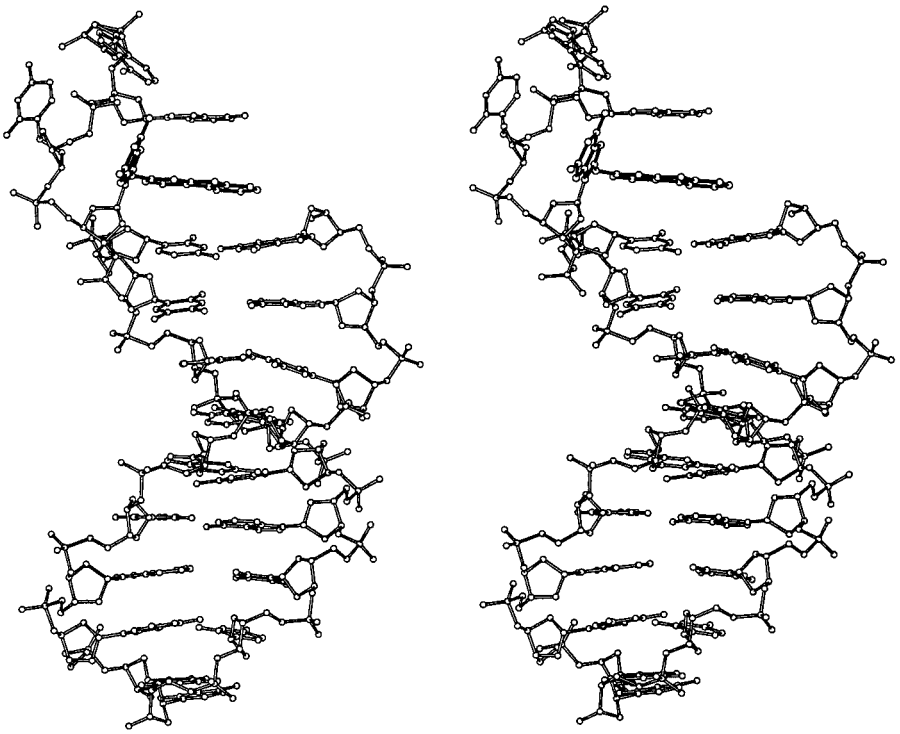

FIGURE 10: Stereo view normal to the helix axis of the representive intensity-refined structure of the entire [AF]dG 13/9-mer duplex. The figure was prepared using Molscript V1.1 (*35*).

and adjacent to the lesion site in the intensity-refined structures of the [AF]dG 13/9-mer are listed in Table S2. The **P** value for dA2 is distinct and spans the range 12 ± 9°, which puts it in the C3′-*endo* range. This conclusion is not supported experimentally since we observe both H1′-H2′ and H1′-H2″ coupling cross-peaks for dA2 that is part of the single strand segment (Figure 5B). It should be noted that the H2′ proton is unexpectedly downfield of its H2″ proton counterpart for dA2 in the [AF]dG 13/9-mer (Table 1 and Figure 5B).

Comparison of First-Stage DUPLEX and Second-Stage X-PLOR Intensity-Refined Structures. The key conformational features centered about the [AF]dG adduct site are shared by both the first-stage DUPLEX (Figure S1) and second-stage X-PLOR intensity-refined (Figures 8 and 9) structures of the [AF]dG 13/9-mer. This includes Watson−Crick alignment of the dC5·dG22 base pair adjacent to the junction site, stacking of aminofluorene ring between the dC5·dG22 and dA2 with its C^9-containing edge facing the major groove, and base displacement of the modified guanine in a *syn* alignment into major groove. Furthermore, the carcinogen−base linkage site torsion angles α′ ([AF]dG4-(N^9)-[AF]dG4(C^8)-[AF](N)-[AF](C^2)) and *β*′ ([AF]dG4(C^8)-[AF](N)-[AF](C^2)-[AF] (C^1)) are 183° and 54°, respectively, for the unrestrained DUPLEX-based structure and are 230.7 ± 27.5° and 10.5 ± 22.8°, respectively, for the X-PLOR-based intensity-refined structures.

Comparison with Structures of [AF]dG in Normal Duplexes and in −1 and −2 Deletion Context. The conformational theme of base displacement of *syn* modified guanine into the major groove accompanied by stacking/intercalation of the fluorene ring with flanking base pairs/bases has proved to be an important concept that has been detected for the [AF]dG adduct in a number of sequence contexts. Thus, this alignment has now been observed in normal duplexes as a contributor to the distribution between AF-intercalated and AF-looped out conformers (*14*, *15*), in the −1 (*4*) and −2 deletion context (*5*, *6*) and in the present single strand−duplex junction context. This structural theme, first proposed by Grunberger et al. (*21*) in the base displacement model for AAF modification and by Fuchs and Daune (*22*) in the insertion−denaturation model, has proved to be remarkably robust. It has also been observed in a normal duplex modified by AAF (*23*) and by 1-aminopyrene (AP) (*8*) and in adducts of benzo[*a*]pyrene (BP) (reviewed in ref 24).

Comparison with Structure of [BP]dG Adduct at a Single Strand−Duplex Junction. There are unexpected similarities between the (+)-*trans-anti*-[BP]dG structure (*2*) (Figure 11A) and the present [AF]dG structure (Figure 11B) when positioned at the same single strand−duplex junctions in the 13/9-mer context. In both cases, the *syn*-modified guanine is displaced into the major groove and is replaced by the carcinogen, which now stacks with the adjacent dC5·dG22 base pair. The major differences are in the alignment of the carcinogen relative to the base pairing axis and the exposure of the unstacked face of the carcinogen to solvent. The C^8-linked [AF]dG adduct is aligned so that the long axis of the fluorenyl ring is parallel to the base pairing axis of the dC5·dG22 pair while the N^2-linked [BP]dG adduct is aligned so that its long axis perpendicular to the dC5·dG22 pairing axis. Furthermore, the BP has its unstacked face exposed to solvent while the AF is partially stacked with the unpaired dA2 and is consequently much less exposed at the single strand−duplex junction.

Biological Implications. The majority of mutations observed following AF modification of guanine are G to T transversions corresponding to [AF]dG·dA mismatch alignment formation (*25*). A *syn* base-displaced AF-inserted structure of the type observed in the present study could certainly be envisioned as miscoding. A rationale for the observed G to T transversions in relation to this structure could involve insertion of adenine opposite the [AF]dG

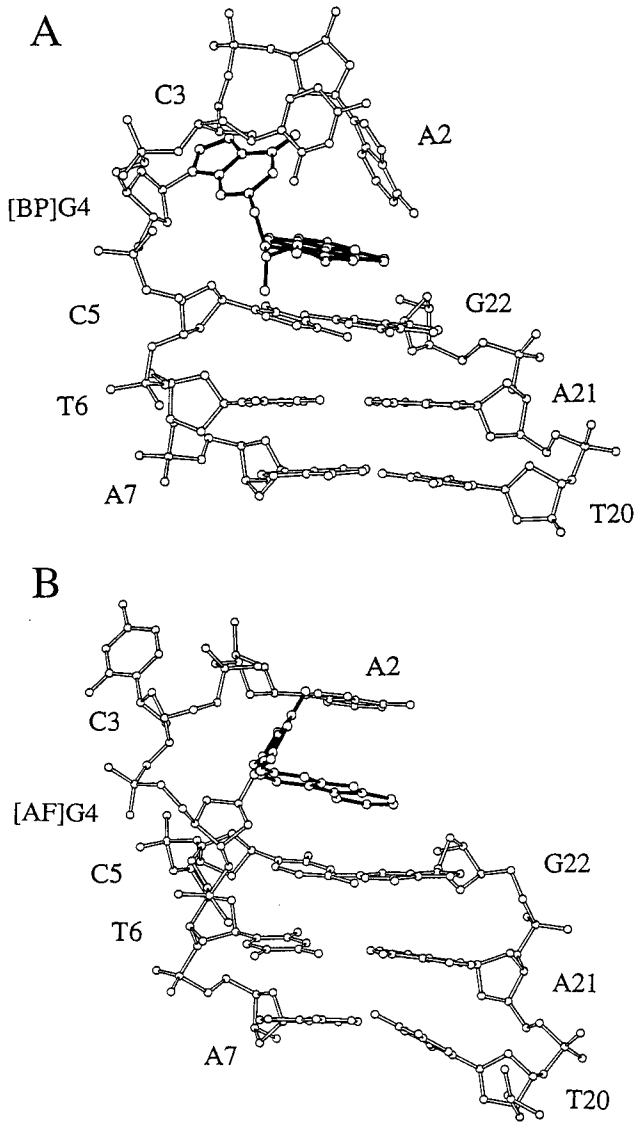

FIGURE 11: Comparision of (A) the 6/3-mer segment of the (+)-*trans-anti*-[BP]dG 13/9-mer structure deduced from an NMR distance-based molecular mechanics refinement characterization (*2*) and (B) the 6/3-mer segment of the [AF]dG 13/9-mer structure deduced from an NMR intensity-based molecular dynamics refinement characterization (this study) in the same sequence context.

facilitated by stabilizing interactions at the template-primer junction or perhaps according to the 'A' rule (*26*). This could be followed by stabilization of the G·A mismatch through a small rearrangement of the *syn*-modified dG and its adducted AF, so as to place the AF in the minor groove position observed in the solution structure of an [AF]dG·dA mismatch in a full duplex (*12*).

A structure such as the one observed in this work could also be envisioned capable of causing polymerase stalling, which could allow time for the formation of a bulged misaligned intermediate in an appropriate sequence (*27*−*30*) that could produce a deletion or an insertion. Both types of mutations are observed to some extent in AF-modified systems (*25*). This is particularly plausible in view of the similarity of key structural features between our structure at this single strand−duplex junction and the one described in the proceeding paper in a bulged −2 deletion duplex (*6*).

Finally, the similarity of certain structural alignments between the C^8-[AF]dG (Figure 11B) and the N^2-(+)-*trans-anti*-[BP]dG (Figure 11A) structures at the single strand−duplex junction reinforces the common principles of base displacement and carcinogen-base stacking. The hypothesis that such a structure may be a common mutagenic conformation at a replication fork was initially based solely on the basis of computational investigations without restraints on these adducts (*31*−*33*). Experimental support for such a concept first emerged from the NMR studies of Eckel and Krugh (*34*) on the [AF]dG adduct system except that they proposed an *anti* alignment for the modified guanine in the AF-intercalated conformer of the [AF]dG adduct positioned opposite dC at the duplex level. The NMR-based solution structures for the [AF]dG (this study) and (+)-*trans-anti*-[BP]dG (*2*) adducts in this model replication intermediate offer experimental views with *syn* alignments for the modified guanines in the carcinogen-intercalated conformers in the template-primer context that is most relevant to mutagenicity.

ACKNOWLEDGMENT

We thank Peter Wei for his technical assistance on this project.

SUPPORTING INFORMATION AVAILABLE

Two tables listing the complete exchangeable and non-exchangeable proton chemical shifts and the sugar pseudorotation and glycosidic torsion angles in the refined structures of the [AF]dG 13/9-mer and one figure showing the superposition of three structures that best fit the NMR data obtained using DUPLEX-based molecular mechanics calculations (5 pages). Ordering information is given on any current masterhead page.

REFERENCES

1. Beland, F. A., and Kadlubar, F. F. (1990) in *Handbook of Experimental Pharmacology, Vol. 94/I*: *Chemical Carcinogenesis and Mutagenesis* (Cooper, C. S., and Grover, P. L., Eds.) pp 267−325, Springer-Verlag, Heidelberg.
2. Cosman, M., Hingerty, B. E., Geacintov, N. E., Broyde, S., and Patel, D. J. (1995) *Biochemistry 34*, 15334−15350.
3. Koehl, P., Valladier, P., Lefevre, J. F., and Fuchs, R. P. P. (1989) *Nucleic Acids Res. 17*, 9531−9541.
4. Mao, B., Cosman, M., Hingerty, B. E., Broyde, S., and Patel, D. J. (1995) *Biochemistry 34*, 6226−6238.
5. Mao, B., Cosman, M., Hingerty, B. E., Broyde, S., and Patel, D. J. (1995) *Biochemistry 34*, 16641−16653.
6. Mao, B., Gorin, A., Gu, Z., Hingerty, B. E., Broyde, S., and Patel, D. J. (1997) *Biochemistry 36*, 14479−14490.
7. Hingerty, B. E., Figueroa, S., Hayden, T., and Broyde, S. (1989) *Biopolymers 28*, 1195−1222.
8. Mao, B., Vyas, R. R., Hingerty, B. E., Broyde, S., Basu, A. K., and Patel, D. J. (1996) *Biochemistry 35*, 12659−12670.
9. Brunger, A. T. (1992) *X-Plor: A system for X-ray Crystallography and NMR*, Yale University Press, New Haven and London.
10. Patel, D. J., Shapiro, L., and Hare, D. (1987) *Annu. Rev. Biophys. Biophys. Chem. 16*, 423−454.
11. van de Ven, F. J., and Hilbers, C. W. (1988) *Eur. J. Biochem. 178*, 1−38.
12. Norman, D., Abuaf, P., Hingerty, B. E., Live, D., Grunberger, D., Broyde, S., and Patel, D. J. (1989) *Biochemistry 28*, 7462−7476.
13. Wang, Y., and Patel, D. J. (1993) *Structure 1*, 263−282.
14. Mao, B., Cosman, M., Hingerty, B. E., Broyde, S., and Patel, D. J. (1997) *Biochemistry* (in press).
15. Mao, B., Cosman, M., Hingerty, B. E., Broyde, S., and Patel, D. J. (1997) *Biochemistry* (in press).
16. Ghose, R., Marino, J. P., Wiberg, K. B., and Prestegard, J. H. (1994) *J. Am. Chem. Soc. 116*, 8827−8828.
17. Greene, K. L., Wang, Y., and Live, D. (1995) *J. Biomol. NMR 5*, 333−338.

18. Arnott, S., Bond, P. J., Selsing, E., and Smith, P. J. (1976) *Nucleic Acids Res. 2*, 2459−2470.
19. Patel, D. J., Kozlowski, S. A., Nordheim, A., and Rich, A. (1982) *Proc. Natl. Acad. Sci. U.S.A. 79*, 1413−1417.
20. Nikonowicz, E. P., and Gorenstein, D. G. (1990) *Biochemistry 29*, 8845−8858.
21. Grunberger, D., Nelson, J. H., Cantor, C., and Weinstein, I. B. (1970) *Proc. Natl. Acad. Sci. U.S.A. 66*, 488−494.
22. Fuchs, R. P. P., and Daune, M. (1971) *FEBS Lett. 14*, 206−208.
23. O'Handley, S. F., Sanford, D. G., Xu, R., Lester, C., Hingerty, B. E., Broyde, S., and Krugh, T. R. (1993) *Biochemistry 32*, 2481−2497.
24. Geacintov, N. E., Cosman, M., Hingerty, B. E., Amin, S., Broyde, S., and Patel, D. J. (1997) *Chem. Res. Toxicol. 10*, 111−146.
25. Heflich, R. H., and Neft, R. E. (1994) *Mutat. Res. 318*, 73−174.
26. Strauss, B. S. (1991) *BioEssays 13*, 79−84.
27. Kunkel, T. A. (1990) *Biochemistry 29*, 8003−8011.
28. Kunkel, T. A. (1992) *J. Biol. Chem. 267*, 18251−18254.
29. Schaaper, R. M., Koffel-Schwartz, N., and Fuchs, R. P. P. (1990) *Carcinogenesis 11*, 1087−1095.
30. Shibutani, S., and Grollman, A. P. (1993) *J. Biol. Chem. 268*, 11703−11710.
31. Broyde, S., and Hingerty, B. E. (1983) *Biopolymers 22*, 2423−2441.
32. Broyde, S., and Hingerty, B. E. (1984) *Ann. N.Y. Acad. Sci. 435*, 119−122.
33. Hingerty, B. E., and Broyde, S. (1986) *J. Biomol. Struct. Dynam. 4*, 365−371.
34. Eckel, L. M., and Krugh, T. R. (1994) *Biochemistry 33*, 13611−13624.
35. Kraulis, P. J. (1991) *J. Appl. Crystallogr. 24*, 946−950.

BI972206R